Geologic controls on phytoplankton elemental composition

Shlomit Sharoni[a,1] and Itay Halevy[a]

[a]Department of Earth and Planetary Sciences, Weizmann Institute of Science, Rehovot 76100, Israel

Edited by Mark Thiemens, Chemistry and Biochemistry, University of California San Diego, La Jolla, CA; received July 19, 2021; accepted November 16, 2021

Planktonic organic matter forms the base of the marine food web, and its nutrient content (C:N:P_{org}) governs material and energy fluxes in the ocean. Over Earth history, C:N:P_{org} had a crucial role in marine metazoan evolution and global biogeochemical dynamics, but the geologic history of C:N:P_{org} is unknown, and it is often regarded constant at the "Redfield" ratio of ∼106:16:1. We calculated C:N:P_{org} through Phanerozoic time by including nutrient- and temperature-dependent C:N:P_{org} parameterizations in a model of the long-timescale biogeochemical cycles. We infer a decrease from high Paleozoic C:P_{org} and N:P_{org} to present-day ratios, which stems from a decrease in the global average temperature and an increase in seawater phosphate availability. These changes in the phytoplankton's growth environment were driven by various Phanerozoic events: specifically, the middle to late Paleozoic expansion of land plants and the Triassic breakup of the supercontinent Pangaea, which increased continental weatherability and the fluxes of weathering-derived phosphate to the oceans. The resulting increase in the nutrient content of planktonic organic matter likely impacted the evolution of marine fauna and global biogeochemistry.

organic matter stoichiometry | C:N:P | marine fauna evolution

The elemental composition of marine primary producers (phytoplankton) is a key governing factor in the evolution of marine fauna and biogeochemical cycling on geologic (million-year and longer) timescales (1–3). As phytoplankton form the base of the marine food web, the molar ratio by which they incorporate essential nutrients, namely nitrogen and phosphorus, relative to carbon (C:N:P_{org}) reflects the quality of the phytoplankton as a food source. Low-quality food, which has high C:N:P_{org}, may limit the growth and reproduction of herbivores, affecting the dynamics and demographics of marine organisms at higher trophic levels (4–8). In contrast, high-quality organic matter with lower C:N:P_{org} allows the consumers to expend less energy on carbon respiration, leaving more energy to evolve traits that facilitate motility, grazing, and reproduction (1, 3, 8). Furthermore, together with the total availability of the limiting nutrient, C:N:P_{org} governs the amount of organic carbon produced in the photic layer by marine primary producers and the amount of dioxygen (O_2) consumed in the deep ocean by respiration. The dynamics of primary production at the ocean surface and respiration in the ocean interior govern the degree of ocean anoxia, and ultimately the burial of organic carbon in sedimentary rocks, which is responsible for the maintenance of O_2 in Earth's atmosphere over geologic time (9–11).

Despite its evolutionary and biogeochemical importance, the geologic history of C:N:P_{org} is poorly constrained, and this ratio is often regarded to have remained constant at its present-day value throughout Phanerozoic Earth history. A part of the reason for this knowledge gap is the absence of a direct proxy for paleo-C:N:P_{org}. Preferential remineralization of phosphorus and nitrogen during burial in sediments alters the primary composition of fresh organic matter and precludes the use of C:N:P_{org} in sedimentary rocks as such a proxy (1, 12, 13).

Present-Day Variability in C:N:P_{org}

In the present ocean, C:N:P_{org} is often considered to have an average value of 106:16:1 (molar ratio), i.e., the "Redfield ratio" (14, 15). However, substantial spatiotemporal C:N:P_{org} variations have been shown to exist, some of which represent variations in the phytoplankton community composition (16–18). For example, C:P_{org} and N:P_{org} in the cold, nutrient-rich, high-latitude oceans are ∼78:1 and ∼13:1, and this may reflect the regional dominance of diatoms, which display lower-than-Redfield N:P_{org} and C:P_{org} (19–21). In contrast, the warm, nutrient-depleted (oligotrophic) midlatitude oceans are characterized by higher-than-Redfield C:P_{org} and N:P_{org} of ∼195:1 and ∼28:1, and this may reflect the regional dominance of cyanobacteria, which display higher-than-Redfield elemental ratios under nutrient-replete conditions (17, 22). Marine C:N:P_{org} may further deviate from the taxon-specific cellular stoichiometry in response to environmental stresses (23, 24). For example, C:P_{org} of some phytoplankton increases under phosphate scarcity, due to substitution of nonphosphorus membrane lipids for phospholipids (25). Irrespective of their exact cause, these large-scale variations in C:N:P_{org} seem to depend on the abiotic environment, that is, on the temperature and phosphate concentration of seawater (17, 26–28). Thus, a change in these environmental parameters in response to geologic drivers is expected to have altered the average C:N:P_{org} of the planktonic biomass over Earth history (2).

Significance

The elemental composition of marine phytoplankton reflects their quality as a food source and regulates the flow of carbon, oxygen, and nutrients between the ocean, atmosphere, and rock reservoirs. Despite this importance, no systematic estimate exists of the geologic history of phytoplankton elemental composition, which is often regarded to have been constant through time, limiting our understanding of evolutionary patterns and global biogeochemistry. Here, using a biogeochemical model forced by geologic and evolutionary events (e.g., the colonization of the continents by plants), we find that the nutrient content of phytoplankton has increased over the last 550 million y of Earth history. This increase in the organic matter nutrient content has likely been important for the evolution of marine fauna.

Author contributions: S.S. and I.H. designed research; S.S. performed research; S.S. analyzed data; and S.S. and I.H. wrote the paper.

The authors declare no competing interest.

This article is a PNAS Direct Submission.

[1]To whom correspondence may be addressed. Email: shlomit.sharoni@weizmann.ac.il.

This article contains supporting information online at https://www.pnas.org/lookup/suppl/doi:10.1073/pnas.2113263118/-/DCSupplemental.

Published December 21, 2021.

Phanerozoic Global Average Temperature and Surface–Ocean Phosphate Concentration

Phytoplankton C:N:P_{org} ratios are thought to depend mostly on the temperature and/or phosphate concentration of the phytoplankton's growth environment (24, 26, 27). Below we review the Phanerozoic trajectories of these variables in response to tectonic and evolutionary forcings, as predicted by a model for the long-term cycles of phosphate, carbon, O_2, and calcium, which is fully described and discussed elsewhere (29). Briefly, the model temperature is mostly affected by volcanic outgassing rates and continental weatherability, which control atmospheric CO_2 concentrations (*SI Appendix*, *SI Text* and Fig. S1). The model surface–ocean phosphate concentration mostly reflects a balance between a phosphate source from continental weathering and phosphate removal by burial in sedimentary rocks, the latter of which depends on the concentration of O_2 in seawater (*SI Appendix*, *SI Text*).

Paleozoic global average temperatures and surface–ocean phosphate concentrations were likely higher and lower than present, respectively (Fig. 1). The model seawater phosphate concentrations are in agreement with the few existing observational constraints and lower than those in most published long-term Earth-system models (*SI Appendix*, *SI Text* and Fig. S2). Both the high Paleozoic temperature and the low surface–ocean phosphate concentrations are an outcome of relatively low continental weatherability in the absence of land plants (29). The extensive root systems of vascular land plants increase fluid infiltration, the surface area of rock exposed to weathering, and the concentration of organic acids in soils, all of which increase continental weatherability (30, 31). Low continental weatherability means that a balance between the long-term carbon sources (outgassing of CO_2) and sinks (the temperature-dependent rate of continental and seafloor weathering) is achieved at a higher temperature (32, 33). Alongside the effect of continental weatherability on the global average temperature, the importance of seafloor weathering (relative to continental weathering) as a source of alkalinity to the ocean is high when continental weatherability is low. Continental weathering is a source of both alkalinity and phosphate, whereas under the oxidizing conditions characteristic of most of Phanerozoic time, seafloor weathering is a source of alkalinity only and possibly even a small phosphate sink (34). Thus, intervals of low continental weatherability, like the early Paleozoic, may have been characterized by lower rates of weathering-derived phosphate delivery to the ocean and generally lower phosphate concentrations (29). This effect may have been compensated by lower-than-present early Paleozoic deep-ocean O_2 concentrations (35, 36). Anoxic basalt weathering has been suggested to be a phosphate source similar to continental weathering (37), and in this case, early Paleozoic seawater phosphate concentrations may have been close to today's, but the global average temperature would have still been high relative to today (*SI Appendix*, *SI Text* and Fig. S3).

Several tectonic and evolutionary events shaped the Phanerozoic trajectories of global average temperature and seawater phosphate concentrations. The expansion of land plants (~400 to 350 Ma) enhanced continental weatherability, leading to a decrease in the global average temperature and an increase in the rate of phosphate supply to the ocean from continental weathering. Assembly of the supercontinent Pangaea in the late Paleozoic and its tenure into the middle Mesozoic likely resulted in higher global average temperatures and lower surface–ocean phosphate concentrations—an outcome of the difficulty of delivering moisture to the continental interior and the resulting low continental weatherability. At the onset of the breakup of Pangaea (~237 Ma) surface–ocean phosphate concentrations rose and global temperature decreased toward their present-day values (Fig. 1).

Here, we explore the effects of these Phanerozoic variations in the marine environment on the evolution of phytoplankton elemental composition. In the model described above, we implemented phosphate- and temperature-dependent C:N:P_{org} parameterizations (*Materials and Methods*) adopted from empirical global-scale relationships (26, 27) and meta-analysis of laboratory culture data (24). Our results suggest a decrease from high Paleozoic C:P_{org} and N:P_{org} to present-day Redfield ratios, which is driven by geologic and biological controls on Earth's surface temperature and the seawater phosphate concentration.

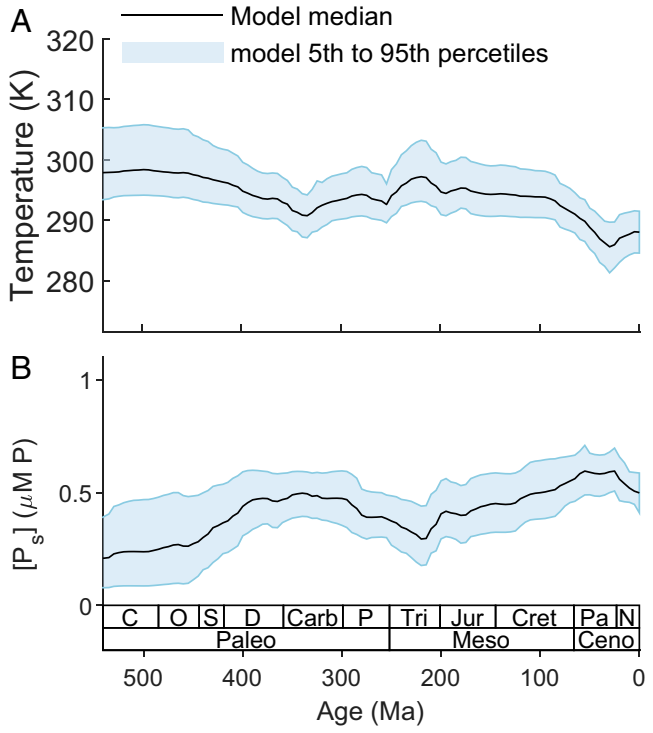

Fig. 1. Global temperature and surface–ocean phosphate concentration throughout the Phanerozoic (adapted from ref. 29). (*A* and *B*) The evolution of (*A*) temperature (K) and (*B*) surface–ocean phosphate concentration (μM P) obtained in ~10^6 default model simulations (5th to 95th percentiles of the results) where input parameters and time-dependent forcings were drawn from probability distributions that represent uncertainty in their values. Adapted from 29.

Results and Discussion

The Evolution of Phytoplankton C:N:P_{org}. The overall evolution of Phanerozoic C:N:P_{org} is a consequence of evolving global temperatures and seawater phosphate concentrations. The effect of these environmental parameters on model phytoplankton C:N:P_{org} is tested using three different empirical relationships (*Materials and Methods*): 1) a field-based phosphate–C:N:P_{org} relationship (26), 2) a field-based temperature–C:N:P_{org} relationship (27), and 3) a laboratory meta-analysis–based temperature– and phosphate–C:N:P_{org} relationships (24). Driven by the Phanerozoic evolution of seawater phosphate concentrations and global average temperatures (Fig. 1), all three parameterizations yield higher-than-Redfield C:P_{org} and N:P_{org} during the early Paleozoic (Fig. 2 *A* and *B*). For example, the temperature-dependent field-based parameterization 2 yields early Paleozoic C:P_{org} between ~130 and 230 and N:P_{org} between ~20 and 30 (95% of model results). If lower deep-ocean O_2 concentrations resulted in a phosphate source from seafloor weathering (e.g., ref. 37), then Paleozoic phosphate concentrations higher than our default scenario would result in

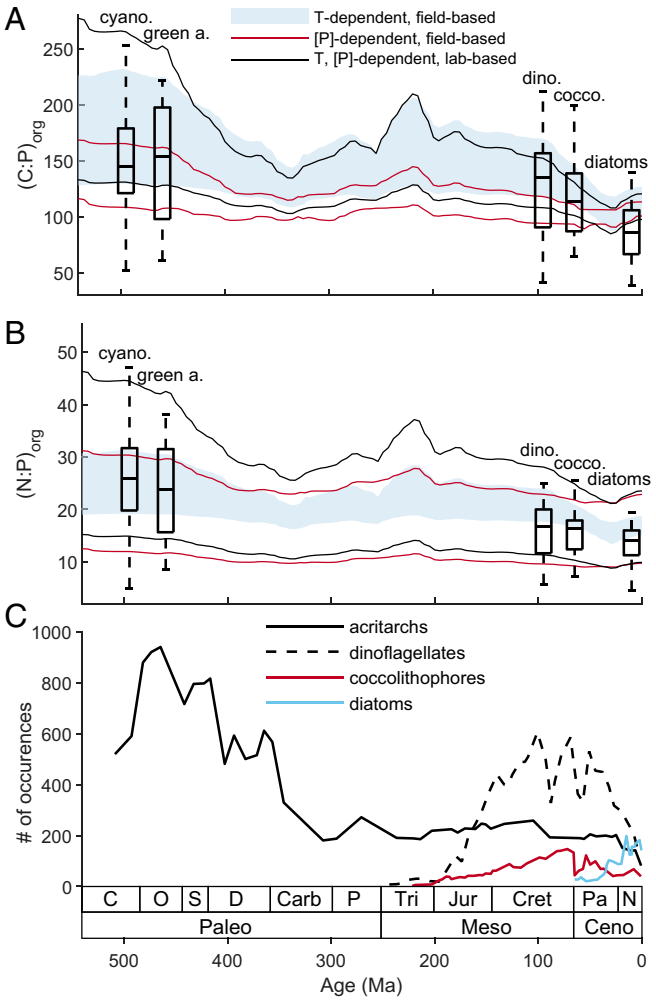

Fig. 2. The evolution of phytoplankton C:N:P_{org}. (*A* and *B*) C:P_{org} (*A*) and N:P_{org} (*B*) (molar ratio) calculated from ~10^6 model simulations (5th to 95th percentiles of the results) where we draw ~37 input parameters and 11 time-dependent forcings from probability distributions that represent uncertainty in their values. The elemental ratios were calculated using three parameterizations for the dependence of C:N:P_{org} on environmental parameters (*Materials and Methods*). Boxplots show the C:P_{org} and N:P_{org} of modern major phytoplankton groups (boxes, 25th, 50th, and 75th percentiles; whiskers, 99.3% of the data) growing under nutrient-replete conditions, plotted against their time of peak occurrence in the fossil record. (*C*) Occurrences of the different phytoplankton groups in the geologic record (*Materials and Methods*).

lower C:P_{org} and N:P_{org}, but only in the phosphate-dependent parameterization 1. Paleozoic temperatures were likely higher irrespective of the role of seafloor weathering in the phosphate cycle, and so the two temperature-dependent parameterizations 2 and 3 consistently yield higher C:P_{org} and N:P_{org} (*SI Appendix*, Fig. S3). The high C:P_{org} values that we predict in the early Paleozoic are in broad agreement with estimates of Precambrian C:P_{org} of 300 to 400 (38), which were calculated on the basis of relations between cyanobacteria-dominated biomass C:N:P_{org} and ambient phosphate concentrations (39).

With all three parameterizations, C:P_{org} and N:P_{org} decreased when green algae colonized the continents (i.e., the evolution of land plants) and enhanced continental weatherability at ~400 to 350 Ma. During the tenure of the supercontinent Pangaea (~300 to 237 Ma), our model predicts an increase in C:P_{org} and N:P_{org} in response to the decrease in continental weatherability and the associated increase in the global average temperature and decrease in the seawater phosphate concentration (Fig. 1). As Pangaea broke apart, our model C:P_{org} and N:P_{org} decline to present-day Redfield values (Fig. 2*A* and *B*). The ratios calculated on the basis of laboratory studies of phytoplankton growing under different degrees of phosphate and temperature limitation (parameterization 3) (24) are consistently highest. Field-based empirical relationships between C:N:P_{org} and sea-surface temperature (parameterization 2) (27) or seawater phosphate concentrations (parameterization 1) (26) yield intermediate and lowest C:N:P_{org} ratios, respectively. The Phanerozoic C:P_{org} and N:P_{org} median values and 95% confidence intervals calculated with all three parameterizations are provided in Zenodo (40).

We compared our calculated C:P_{org} and N:P_{org} with observed C:P_{org} and N:P_{org} of modern representatives of the major phytoplankton groups. The phytoplankton group-specific C:P_{org} and N:P_{org} values are derived from laboratory strains growing under nutrient-replete conditions (18), which show that red algae tend to thrive under nutrient-rich conditions and display lower C:P_{org} and N:P_{org} than their green and cyanobacterial counterparts (19–21). The group-specific C:P_{org} and N:P_{org} values are plotted against the group's time of peak appearance in the fossil record (Fig. 2). Although molecular clock analyses suggest that the three principal red-taxa phytoplankton groups (dinoflagellates, coccolithophores, and diatoms) evolved before the Paleozoic (41, 42), the fossil record indicates that these groups rose to ecological prominence only during the Mesozoic (Fig. 2*C*). Prior to the Mesozoic, evidence suggests that the green superfamily and cyanobacteria dominated marine primary production (43–47).

Model C:P_{org} and N:P_{org} at the time of the major phytoplankton groups' peak appearance are similar to C:P_{org} and N:P_{org} in modern representatives of those groups, grown under nutrient-replete conditions (Fig. 2). Application of relationships from the modern ocean to the geologic past carries uncertainty. However, the favorable comparison of our results with the microfossil record suggests that nutrient preferences and elemental compositions of modern phytoplankton groups may be conserved traits that reflect their inherent physiology (21, 48), rather than evolutionary adaptations to the modern marine nutrient regime. If correct, this means, for example, that cyanobacteria have not evolved to thrive at the low nutrient levels in the oligotrophic gyres, in response to the colonization of high-nutrient waters by modern phytoplankton. Instead, cyanobacteria have always been well suited to the low nutrient levels prevalent during their emergence, and they currently occupy the environments remaining to them—oligotrophic waters unsuited for growth of the more nutrient-rich modern taxa. The conclusion that the elemental composition of phytoplankton is constrained by genetics and evolutionary history is supported by the observation that cyanobacterial strains that have been cultivated under nutrient-replete conditions for almost 40 y still retain a high C:N:P_{org} (21, 22). Given the short generation time of cyanobacteria (approximately two divisions per day), this duration of cultivation is one to two orders of magnitude longer than that required for adaptive evolution (49).

Higher early Paleozoic C:P_{org} and N:P_{org} values are also consistent with the low suggested "energetics" (biomass, metabolic rates, and physical activity, such as motility and predation) of marine fauna of that time (1, 45, 50–54). On a high C:P_{org} diet (i.e., low-quality food), the energy spent on carbon respiration to access nutrients limits the energy available to evolve traits that facilitate motility, grazing, and reproduction (1, 3, 8). Most Paleozoic fauna fed close to the sediment–water interface and appear to have been characterized by low metabolic and diversification rates (52). Predation and bioturbation, which require substantial amounts of energy (for more advanced nervous and muscular systems), appear to have become more common through time, especially during the Meso-Cenozoic (54, 55), perhaps indicating

that food quality increased (i.e., $C:P_{org}$ and $N:P_{org}$ decreased) around that time.

Biogeochemical Implications of Higher Paleozoic $C:P_{org}$. Phytoplankton elemental composition has been frequently assumed to be constant at the Redfield ratio in studies of the long-term biogeochemical cycles. However, our study suggests higher-than-Redfield $C:P_{org}$ and $N:P_{org}$ during the early Paleozoic, driven by lower phosphate concentrations and a higher temperature. Persistently high Paleozoic $C:P_{org}$ (Fig. 3*A*), produced by plasticity in the elemental composition of phytoplankton biomass, would have had significant consequences for marine biogeochemical cycling. For example, early Paleozoic carbon-based new production and burial of organic carbon are higher at elevated $C:P_{org}$ relative to the case with a Redfield $C:P_{org}$ (Fig. 3 *B* and *C*), and this leads to higher atmospheric pO_2 (Fig. 3*E*). Although O_2 production rates in the surface ocean are expected to be higher at elevated $C:P_{org}$ (relative to a Redfield $C:P_{org}$), so is export of organic carbon from the surface to the deep ocean. The associated consumption of O_2 in the deep ocean results in lower deep-ocean O_2 concentrations (Fig. 3*F*), likely leading to more widespread anoxia. This is in accordance with proxy-based suggestions of deep-ocean anoxia persisting into the middle Paleozoic (35, 56, 57). In contrast to a pronounced effect on the organic carbon and O_2 cycles, our model predicts that the long-term inorganic carbon cycle is not affected by the introduction of flexible $C:N:P_{org}$ (Fig. 3 *G* and *H*, all lines overlap). Atmospheric pCO_2 and the global average surface temperature are insensitive to $C:N:P_{org}$ because the enhanced burial of organic carbon at high $C:P_{org}$ is compensated by larger oxidative weathering fluxes of sedimentary organic matter. The increase in organic carbon weathering arises from the increase in atmospheric pO_2, which is a consequence of the enhanced organic carbon burial (Fig. 3*D*).

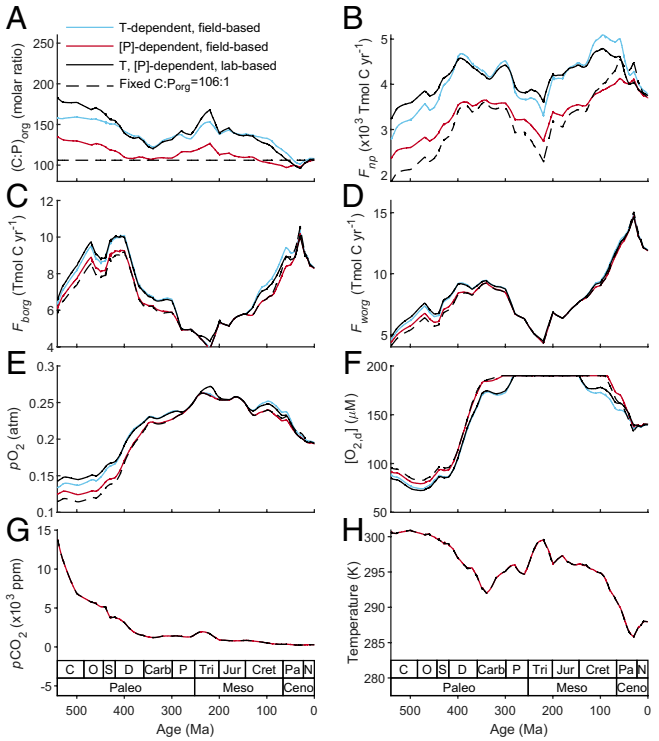

Fig. 3. Effects of the proposed Phanerozoic evolution of $C:N:P_{org}$ on the carbon and O_2 cycles. (*A–H*) Comparison between (*A*) $C:P_{org}$ (molar ratio), (*B*) carbon-based primary productivity ($\times 10^3$ Tmol C $\times$ y^{-1}), (*C*) marine organic carbon burial (Tmol C $\times$ y^{-1}), (*D*) weathering of organic matter in sedimentary rocks (Tmol C $\times$ y^{-1}), (*E*) atmospheric pO_2 (atm), (*F*) the deep-ocean O_2 concentration (μM), (*G*) atmospheric pCO_2 ($\times 10^3$ ppm), and (*H*) temperature (K), for $C:N:P_{org}$ that is fixed at the Redfield ratio (dashed black line) or variable according to the three parameterizations presented in Fig. 2.

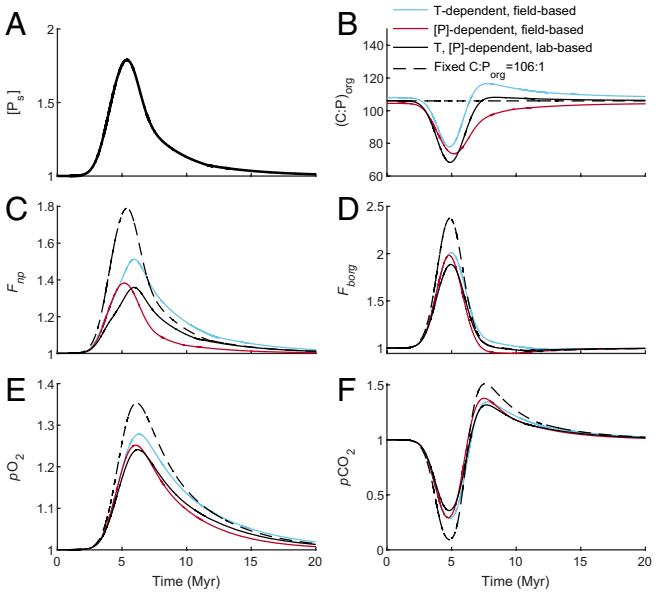

Fig. 4. Dynamic response of model variables to an increase in the phosphate delivery rate at a constant (Redfield) and variable $C:N:P_{org}$. (*A–F*) Surface phosphate concentration (forcing function) (*A*), $C:P_{org}$ of the primary producers (mol C $\times$mol P^{-1}) (*B*), carbon-based primary productivity (*C*), burial of organic carbon (*D*), atmospheric pO_2 (*E*), and atmospheric pCO_2 (*F*). All fluxes and pools are normalized to present-day values and are unitless.

The compensating effects of organic carbon burial and oxidative weathering on the inorganic carbon cycle and temperature, described above, operate on the timescale of formation, burial, uplift, and weathering of sedimentary rocks (i.e., tens of millions of years or more). On shorter timescales, before the sedimentary organic matter pool has fully adjusted to a change in the surface environment, we find that flexible $C:P_{org}$ stabilizes the organic and inorganic carbon cycles and the O_2 cycle, similar to the findings of previous studies (26, 58). Upon perturbation of phosphate supply rates, e.g., by continental flooding or the development of anoxic basins, a rigid coupling (i.e., fixed $C:P_{org}$) leads to a stronger response of organic carbon burial, CO_2 drawdown, and O_2 production and release to the atmosphere. During a phosphate enrichment event (Fig. 4*A*), when $C:P_{org}$ is fixed at the Redfield ratio (Fig. 4*B*), more carbon is fixed by marine primary producers, and as a result organic carbon burial and pO_2 transiently reach higher values than in the case of flexible $C:P_{org}$ (Fig. 4 *C–E*). The higher rates of organic carbon burial shuttle carbon from the ocean–atmosphere into marine sediments, and pCO_2 drops substantially (Fig. 4*F*). The pCO_2 drop is significantly larger when $C:P_{org}$ is fixed at the Redfield ratio, resulting in global cooling.

Conclusions

We constrained the elemental composition of marine biomass through Phanerozoic time by including phosphate- and temperature-dependent parameterizations of $C:N:P_{org}$ in a long-term biogeochemical model. We infer a decrease from high Paleozoic $C:P_{org}$ and $N:P_{org}$ to present-day Redfield ratios. The decrease in $C:P_{org}$ and $N:P_{org}$ is a result of a decrease in surface temperature and an increase in phosphate availability in the ocean, driven mainly by the emergence and expansion of land plants in the middle to late Paleozoic and by the Triassic breakup of the supercontinent Pangaea. Our results are consistent with the evolutionary trajectory of phytoplankton and with an increase in the energetics of marine fauna suggested by the fossil record.

Our time-dependent C:N:P_{org} at the times of peak appearance of the major phytoplankton groups is consistent with that of modern representatives of those groups. This suggests that the elemental composition of these phytoplankton groups is a conserved trait, which is constrained by genetics and evolutionary history, and not an acquired trait. These ideas may be taken a (speculative) step farther. Although uncertainty exists in the reasons and exact timing of evolution and emergence to prominence of the different phytoplankton groups, we raise the possibility that the more nutrient-rich red-lineage phytoplankton were driven to dominance by the shifts in nutrient availability and climate that we describe above. This suggests a link between evolution and tectonics.

We further explored the biogeochemical consequences of flexible elemental ratios on the carbon and O_2 cycles. Our results suggest that the higher-than-Redfield C:P_{org} likely prevalent during the early Phanerozoic led to higher marine primary productivity and organic carbon burial, relative to the case of a time-invariant C:P_{org}. This simultaneously leads to higher atmospheric O_2 levels and more extensive anoxia in the ocean interior, relative to the case of a constant, Redfield C:P_{org}. Finally, on short timescales, we find that flexible C:P_{org} weakens the coupling between the phosphorous, carbon, and O_2 cycles and dampens perturbations in the carbon and O_2 cycles driven by changes in the rate of phosphate delivery to the ocean (Fig. 4).

In summary, it seems that flexibility in the elemental composition of phytoplankton biomass has led to a Phanerozoic decrease in C:P_{org} and N:P_{org} in response to tectonic and evolutionary drivers. This long-term decrease in C:P_{org} and N:P_{org} affected biogeochemical cycling and the stability of Earth's atmospheric composition and climate over Phanerozoic time.

Materials and Methods

Experiments and Numerical Solution. To explore the possibility that the elemental composition of planktonic organic matter varied through time, we implemented nutrient- and temperature-dependent C:N:P_{org} parameterizations in a model for the long-term cycles of phosphate, carbon, O_2, and calcium (the model development, validation, and the numerical procedure are fully described in ref. 29). We tested the evolution of C:N:P_{org} in four experiments. In one, C:N:P_{org} was fixed at the Redfield ratio of 106:16:1. In three others, C:N:P_{org} depended on environmental parameters, as described below. In each experiment we performed $\sim 10^6$ simulations, where we randomly drew 36 to 37 parameters and 11 time-dependent forcings from distributions that represent the uncertainty in their values (34 parameters are associated with the original model described in ref. 29, and 2 to 3 additional parameters are associated with each C:N:P_{org} parameterization; Table 1).

Flexible elemental ratios in marine organic matter over Phanerozoic time are calculated in our model using three different relationships between C:N:P_{org} and the abiotic environment. The C:N:P_{org} parameterization 1 is based on an empirical global relationship between C:N:P_{org} and surface phosphate concentrations in the ocean (26): $(P:C)_{org} = (\rho_1 \times [P]_s + \rho_2)$, where ρ_1 and ρ_2 are parameters that characterize the linear geographic $(P:C)_{org}$ dependence on surface phosphate concentrations. The intercept, ρ_2, which corresponds to the lowest P:C_{org}, is between 0.0048 and 0.006 (based on binned or unbinned regressions, respectively; figure S2 in ref. 26), and we adopted this range (Table 1). To normalize to present-day conditions, where at the global average surface phosphate concentration $[P]_s^0 = 0.5\ \mu M$, P:C_{org} is at the Redfield ratio (P:$C^0_{org} = 0.0094$), we set $\rho_1 = \left(\frac{\rho_2 - 0.0094}{-0.5}\right)$. To calculate N:$P_{org}$ we substitute $(N:P)_{org} = (C:P)_{org}/(C:N)_{org}$. As C:$N_{org}$ is relatively uniform across oceanic regions (26) and among different phytoplankton taxa (23), we draw it from a distribution that represents the variability in this value across different phytoplankton taxa growing under nutrient-replete conditions (Table 1).

Parameterization 2 is based on observed correlations between surface C:N:P_{org} in the present ocean and sea-surface temperature (27). The geographic temperature dependence of algal elemental composition is given by the equations $(C:P)_{org} = (C:P)^0_{org} \times e^{\rho_3\left(T - T^0\right)}$ and $(N:P)_{org} = (N:P)^0_{org} \times e^{\rho_4\left(T - T^0\right)}$, where $(C:P)^0_{org}$, $(N:P)^0_{org}$ are the Redfield ratios, ρ_3 and ρ_4 are parameters that characterize the geographic temperature dependence (Table 1), and T is the global average surface temperature in Kelvins (T^0 is the present-day temperature).

Parameterization 3 is based on a meta-analysis of laboratory experimental data, where the following relationship was reported: $(P:C)_{org} = (P:C)^0_{org} \times \left(\frac{[P]_s}{[P]^0_s}\right)^{\rho_5} \times \left(\frac{T}{T^0}\right)^{\rho_6}$. Here, ρ_5 and ρ_6 are empirical parameters that represent the sensitivity of the P:C_{org} of different phytoplankton groups to the phosphate concentration and temperature, respectively. We used cyanobacterial $\rho_5 = 0.3$ and $\rho_6 = -7.8$ parameters (Table 1), but note that using eukaryote parameters ($\rho_5 = 0.4$ and $\rho_6 = 0$) would give similar results due to a tradeoff between phosphate and temperature acclimation (24).

Table 1. C:N:P_{org} parameterizations employed in this study

Symbol	Range	Distribution*	Ref.
ρ_1	$\rho_1 = \left(\frac{\rho_2 - 0.0094}{-0.5}\right)$		(26)
ρ_2	0.0048 to 0.006	Uniform	(26)
C:N_{org}	1.961 (0.256)	Lognormal	(18)
ρ_3	0.037 (0.010)	Normal	(27)
ρ_4	0.032 (0.008)	Normal	(27)
ρ_5	0.29 (0.8)	Normal	(24)
ρ_6	−7.8 (0.8)	Normal	(24)
C:P^0_{org}	106		
C:N^0_{org}	16		

*For normal and lognormal distributions, numbers outside and inside the parentheses represent the mean and SD, respectively.

Fossil Assemblage. The fossil data in Fig. 2*C* represent the number of occurrences of the different phytoplankton groups in the geologic record, which were compiled from the Paleobiology database (https://paleobiodb.org) using the following parameters: time intervals = Phanerozoic, paleoenvironment = marine, order = acritarchs, prymnesiophycea, dinophycea, diatoms). Acritarchs are considered to include the earliest green algae, which use chlorophyll-b. Dinoflagellates, coccolithophores, and diatoms, i.e., "modern" red phytoplankton groups, use chlorophyll-c. Biomarkers suggest that cyanobacteria played a significant role in Paleozoic marine primary production alongside green algae (46), and we, therefore, show the elemental composition of cyanobacteria in Fig. 2 *A* and *B* in the early Paleozoic.

Data Availability. The code used in this study and the model C:Porg and N:Porg trajectories (medians and 95% confidence intervals) over Phanerozoic time are provided in Zenodo (https://zenodo.org/record/5768279#.YbttQWjMKHs; ref. 40). All study data are included in this article and/or *SI Appendix*.

ACKNOWLEDGMENTS. We thank the Interuniversity Institute for Marine Sciences in Eilat, Israel for hosting S.S. S.S. acknowledges support from the Rieger Foundation of the Jewish National Fund and a Pearlman Grant for Student-Initiated Research from the Weizmann Institute of Science.

1. R. E. Martin, A. Quigg, V. Podkovyrov, Marine biodiversification in response to evolving phytoplankton stoichiometry. *Palaeogeogr. Palaeoclimatol. Palaeoecol.* **258**, 277–291 (2008).
2. N. J. Planavsky, The elements of marine life. *Nat. Geosci.* **7**, 855–856 (2014).
3. R. E. Martin, T. Servais, Did the evolution of the phytoplankton fuel the diversification of the marine biosphere? *Lethaia* **53**, 5–31 (2020).
4. A. M. Malzahn, N. Aberle, C. Clemmesen, M. Boersma, Nutrient limitation of primary producers affects planktivorous fish condition. *Limnol. Oceanogr.* **52**, 2062–2071 (2007).
5. D. M. Ware, R. E. Thomson, Bottom-up ecosystem trophic dynamics determine fish production in the Northeast Pacific. *Science* **308**, 1280–1284 (2005).
6. E. M. Dickman, J. M. Newell, M. J. González, M. J. Vanni, Light, nutrients, and food-chain length constrain planktonic energy transfer efficiency across multiple trophic levels. *Proc. Natl. Acad. Sci. U.S.A.* **105**, 18408–18412 (2008).
7. S. J. Moe *et al.*, Recent advances in ecological stoichiometry: Insights for population and community ecology. *Oikos* **109**, 29–39 (2005).
8. R. W. Sterner, J. J. Elser, *Ecological Stoichiometry: The Biology of Elements from Molecules to the Biosphere* (Princeton University Press, 2002).
9. T. Volk, M. I. Hoffert, "Ocean carbon pumps: Analysis of relative strengths and efficiencies in ocean-driven atmospheric co_2 changes" in *The Carbon Cycle and Atmospheric CO_2: Natural Variations Archean to Present*, E. Sundquist, W. Broecker, Eds. (Wiley Online Library, 1985), **vol. 32**, pp. 99–110.

10. W. S. Broecker, G. M. Henderson, The sequence of events surrounding Termination II and their implications for the cause of glacial-interglacial CO_2 changes. *Paleoceanography* **13**, 352–364 (1998).
11. R. A. Berner, A model for calcium, magnesium and sulfate in seawater over Phanerozoic time. *Am. J. Sci.* **304**, 438–453 (2004).
12. K. L. Faul, A. Paytan, M. L. Delaney, Phosphorus distribution in sinking oceanic particulate matter. *Mar. Chem.* **97**, 307–333 (2005).
13. G. Lyons, C. R. Benitez-Nelson, R. C. Thunell, Phosphorus composition of sinking particles in the Guaymas Basin, Gulf of California. *Limnol. Oceanogr.* **56**, 1093–1105 (2011).
14. A. C. Redfield, "On the proportions of organic derivatives in sea water and their relation to the composition of plankton" in *James Johnstone Memorial Volume*, R. J. Daniel, Ed. (University Press of Liverpool, 1934), pp. 176–192.
15. A. C. Redfield, The biological control of chemical factors in the environment. *Am. Sci.* **46**, 205–221, 230A (1958).
16. K. R. Arrigo, Marine microorganisms and global nutrient cycles. *Nature* **437**, 349–355 (2005).
17. A. C. Martiny *et al.*, Strong latitudinal patterns in the elemental ratios of marine plankton and organic matter. *Nat. Geosci.* **6**, 279–283 (2013).
18. S. Sharoni, I. Halevy, Nutrient ratios in marine particulate organic matter are predicted by the population structure of well-adapted phytoplankton. *Sci. Adv.* **6**, eaaw9371 (2020).
19. A. Quigg *et al.*, The evolutionary inheritance of elemental stoichiometry in marine phytoplankton. *Nature* **425**, 291–294 (2003).
20. T. Ho *et al.*, The elemental composition of some marine phytoplankton. *J. Phycol.* **39**, 1145–1159 (2003).
21. A. Quigg, A. J. Irwin, Z. V. Finkel, Evolutionary inheritance of elemental stoichiometry in phytoplankton. *Proc. Biol. Sci.* **278**, 526–534 (2011).
22. S. Bertilsson, O. Berglund, D. M. Karl, S. W. Chisholm, Elemental composition of marine prochlorococcus and synechococcus: Implications for the ecological stoichiometry of the sea. *Limnol. Oceanogr.* **48**, 1721–1731 (2003).
23. R. J. Geider, J. La Roche, Redfield revisited: Variability of C:N:P in marine microalgae and its biochemical basis. *Eur. J. Phycol.* **37**, 1–17 (2002).
24. T. Tanioka, K. Matsumoto, A meta-analysis on environmental drivers of marine phytoplankton C:N:P. *Biogeosciences* **17**, 1–49 (2019).
25. B. A. Van Mooy *et al.*, Phytoplankton in the ocean use non-phosphorus lipids in response to phosphorus scarcity. *Nature* **458**, 69–72 (2009).
26. E. D. Galbraith, A. C. Martiny, A simple nutrient-dependence mechanism for predicting the stoichiometry of marine ecosystems. *Proc. Natl. Acad. Sci. U.S.A.* **112**, 8199–8204 (2015).
27. G. Yvon-Durocher, M. Dossena, M. Trimmer, G. Woodward, A. P. Allen, Temperature and the biogeography of algal stoichiometry. *Glob. Ecol. Biogeogr.* **24**, 562–570 (2015).
28. T. S. Weber, C. Deutsch, Ocean nutrient ratios governed by plankton biogeography. *Nature* **467**, 550–554 (2010).
29. S. Sharoni, I. Halevy, Weathering controls on the phanerozoic phosphate cycle. Research Square [Preprint] (2021). https://www.researchsquare.com/article/rs-618748/v1 (Accessed July 2021).
30. P. Kenrick, C. H. Wellman, H. Schneider, G. D. Edgecombe, A timeline for terrestrialization: Consequences for the carbon cycle in the Palaeozoic. *Philos. Trans. R. Soc. Lond. B Biol. Sci.* **367**, 519–536 (2012).
31. L. L. Taylor *et al.*, Biological weathering and the long-term carbon cycle: Integrating mycorrhizal evolution and function into the current paradigm. *Geobiology* **7**, 171–191 (2009).
32. J. C. Walker, P. Hays, J. F. Kasting, A negative feedback mechanism for the long-term stabilization of Earth's surface temperature. *J. Geophys. Res. Oceans* **86**, 9776–9782 (1981).
33. R. A. Berner, A. C. Lasaga, R. M. Garrels, The carbonate-silicate geochemical cycle and its effect on atmospheric carbon dioxide over the past 100 million years. *Am. J. Sci.* **283**, 641–683 (1983).
34. C. G. Wheat, R. A. Feely, M. J. Mottl, Phosphate removal by oceanic hydrothermal processes: An update of the phosphorus budget in the oceans. *Geochim. Cosmochim. Acta* **60**, 3593–3608 (1996).
35. E. A. Sperling *et al.*, Statistical analysis of iron geochemical data suggests limited late Proterozoic oxygenation. *Nature* **523**, 451–454 (2015).
36. D. A. Stolper, C. B. Keller, A record of deep-ocean dissolved O_2 from the oxidation state of iron in submarine basalts. *Nature* **553**, 323–327 (2018).
37. D. Syverson *et al.*, Nutrient supply to planetary biospheres from anoxic weathering of mafic oceanic crust. *Geophys. Res. Lett.* **48**, e2021GL094442 (2021).
38. C. T. Reinhard *et al.*, Evolution of the global phosphorus cycle. *Nature* **541**, 386–389 (2017).
39. I. Kuznetsov, T. Neumann, H. Burchard, Model study on the ecosystem impact of a variable C:N:P ratio for cyanobacteria in the Baltic Proper. *Ecol. Modell.* **219**, 107–114 (2008).
40. S. Sharoni, I. Halevy , Geologic controls on phytoplankton elemental composition. Zenodo. https://zenodo.org/deposit/5768279. Deposited 8 December 2021.
41. H. S. Yoon, J. D. Hackett, C. Ciniglia, G. Pinto, D. Bhattacharya, A molecular timeline for the origin of photosynthetic eukaryotes. *Mol. Biol. Evol.* **21**, 809–818 (2004).
42. C. De Vargas, M. P. Aubry, I. Probert, J. Young, "Origin and evolution of coccolithophores: From coastal hunters to oceanic farmers" in *Evolution of Primary Producers in the Sea*, P. G. Falkowski, A. H. Knoll, Eds. (Elsevier, 2007), pp. 251–285.
43. H. Tappan, Phytoplankton: Below the salt at the global table. *J. Paleontol.* **60**, 545–554 (1986).
44. P. G. Falkowski *et al.*, The evolution of modern eukaryotic phytoplankton. *Science* **305**, 354–360 (2004).
45. M. E. Katz, Z. V. Finkel, D. Grzebyk, A. H. Knoll, P. G. Falkowski, Evolutionary trajectories and biogeochemical impacts of marine eukaryotic phytoplankton. *Annu. Rev. Ecol. Evol. Syst.* **35**, 523–556 (2004).
46. A. H. Knoll, R. E. Summons, J. R. Waldbauer, J. E. Zumberge, "The geological succession of primary producers in the oceans" in *Evolution of Primary Producers in the Sea*, P. G. Falkowski, A. H. Knoll, Eds. (Elsevier, 2007), pp. 133–163.
47. A. H. Knoll, Paleobiological perspectives on early eukaryotic evolution. *Cold Spring Harb. Perspect. Biol.* **6**, a016121 (2014).
48. E. Litchman, C. A. Klausmeier, Trait-based community ecology of phytoplankton. *Annu. Rev. Ecol. Evol. Syst.* **39**, 615–639 (2008).
49. T. B. Reusch, P. W. Boyd, Experimental evolution meets marine phytoplankton. *Evolution* **67**, 1849–1859 (2013).
50. G. J. Vermeij, The Mesozoic marine revolution: Evidence from snails, predators and grazers. *Paleobiology* **3**, 245–258 (1977).
51. R. K. Bambach, Seafood through time: Changes in biomass, energetics, and productivity in the marine ecosystem. *Paleobiology* **19**, 372–397 (1993).
52. R. K. Bambach, Energetics in the global marine fauna: A connection between terrestrial diversification and change in the marine biosphere. *Geobios* **32**, 131–144 (1999).
53. R. E. Martin, Secular increase in nutrient levels through the Phanerozoic: Implications for productivity, biomass, and diversity of the marine biosphere. *Palaios* **11**, 209–219 (1996).
54. R. E. Martin, A. Quigg, Evolving phytoplankton stoichiometry fueled diversification of the marine biosphere. *Geosciences* **2**, 130–146 (2012).
55. C. W. Thayer, "Sediment-mediated biological disturbance and the evolution of marine benthos" in *Biotic Interactions in Recent and Fossil Benthic Communities*, M. J. S. Tevesz, P. L. McCall, Eds. (Springer, 1983), pp. 479–625.
56. I. J. Glasspool, D. Edwards, L. Axe, Charcoal in the Silurian as evidence for the earliest wildfire. *Geology* **32**, 381–383 (2004).
57. T. W. Dahl *et al.*, Devonian rise in atmospheric oxygen correlated to the radiations of terrestrial plants and large predatory fish. *Proc. Natl. Acad. Sci. U.S.A.* **107**, 17911–17915 (2010).
58. K. Matsumoto, R. Rickaby, T. Tanioka, Carbon export buffering and CO_2 drawdown by flexible phytoplankton C:N:P under glacial conditions. *Paleoceanogr. Paleoclimatol.* **35**, e2019PA003823 (2020).